A Study of Power Electronic Based Stall and Electromechanical Yaw Power Control Strategies in Small-Scale Grid-Connected Wind Turbines

Ebrahim Mohammadi, Roohollah Fadaeinedjad
Dept. of Electrical and Computer Engineering
Graduate University of Advanced Technology
Kerman, Iran
e.mohamadi@ieee.org, rfadaein@kgut.ac.ir

Gerry Moschopoulos
Dept. of Electrical and Computer Engineering
University of Western Ontario
London, Canada
gmoschop@uwo.ca

***Abstract*—The performance of two different control strategies for small-scale squirrel cage induction generator (SCIG) based variable speed wind turbines (WTs) are examined in this paper. The first is stall control, which uses power electronics to force the turbine blades to operate in a stall condition when the turbine is operating in above rated wind speed conditions. The second is yaw control, which rotates the wind turbine away from the direction of the wind to limit power when the turbine is operating above rated wind speed conditions. This paper analyses the performance of these two control strategies and their impact on the utility grid using a comprehensive model that considers electrical, mechanical and aerodynamic aspects of WT operation; the model is discussed in detail in the paper. The comparison shows that completely power electronic-based stall control is better than electromechanical yaw control in terms of power, voltage regulation, and flicker emission level.**

Keywords— Wind energy systems, stall control; yaw control, flicker emission, electromechanical simulation

I. INTRODUCTION

Small-scale variable speed wind turbines (WTs) are widely used in various industrial applications such as water pumping systems, remote site and village electrification and battery chargers [1]. A WT has three main operating regions:

- Region 1 where it is either not rotating at all or is in the process of starting up.
- Region 2 where it is operating at below rated wind speed.
- Region 3 where it is operating above rated wind speed.

For Region 2 operation, maximum power point tracking (MPPT) control strategies are used to extract as much power as possible from the wind. Various MPPT methods have been proposed, including tip speed ratio (TSR) algorithms [2], power signal feedback methods [3], techniques based on optimal torque [4], hill climbing search [5] and incremental conductance MPPT algorithms [6].

For Region 3 operation, the power extracted from the wind needs to be limited and this can be done with various mechanical control strategies such as pitch angle control [7], yaw [8], furl [9], and stall [10] control methods, which limit the speed of mechanical rotation of the turbine. Pitch angle control is mainly used in large-scale WTs due to costs and thus will not be considered in this paper. Furl control involves turning the WT's nacelle at an angle out of the wind direction so that its rotor speed will slow down. Stall control uses power electronics to control the WT generator rotation speed so that the blades are made to stall, thus reducing the amount of power extracted from the wind.

The design of the WT blade is important in stall control, which must consider aerodynamic factors that will allow the WT's speed of rotation to slow down in conjunction with the power electronics. For yaw control (where yaw is the vertical axis of the WT), the yaw mechanism should be designed so that the WT rotor axis is aligned in the direction of the wind (thus making the yaw error zero) under below rated wind speed conditions and less aligned as the WT is rotated out of the wind direction at above rated wind speed operation to limit the extracted power.

There has been little research on the operation of small-scale WTs in Region 3 because of the wide range of expertise needed. Unlike Region 2 operation, for which expertise mainly in electrical engineering is required as the control is electrical, the study of Region 3 operation requires expertise in electrical, mechanical, and aerodynamic engineering since the control depends on all these factors; few research groups have such a combination of expertise.

In [11], an aeroelastic model using FAST and ADAMS codes was developed and used to study the performance of a wind energy system (WES) with a small furl controlled WT. In [9] the performance of a 10 kW furl controlled WT operating under normal and fault ride-through conditions was examined. The performance of furl and stall control strategies were compared in [12] and it was determined that stall control results in greater energy production at high wind speeds and less thrusts and furling noise. In [13], the output power of the stall- and yaw-controlled WTs was compared where the first one demonstrated a better performance and lower power fluctuations.

978-1-5386-1180-7/18/$31.00 ©2018 IEEE

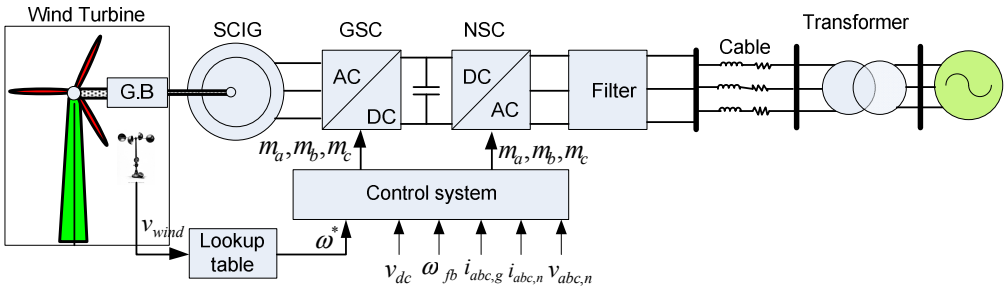

Fig. 1. System configuration

In this paper, a comparison between power electronic based stall control and electromechanical yaw control is made. This paper analyses the performance of these two control strategies and their impact on the grid by using a simulation model that considers the electrical, mechanical and aerodynamic aspects of WT operation; all aspects of the model are discussed in detail in the paper. Results from models of two 10 kW WTs operating with stall control and yaw control are presented and the performance of the WTs are considered with respect to power, voltage regulation and flicker emission level. Conclusions about the two control methods are made based on the simulation work.

II. System Configuration and Simulation Platform

A. System Configuration

The configuration of the 10 kW SCIG-based variable speed WT that is used to study both stall and yaw control is shown in Fig. 1. It is connected to the AC grid through back to back converters, a generator side converter (GSC) and a network side converter (NSC), a filter and network connection. Key WT parameters are sensed, fed to a lookup table, then processed by a controller that controls the converters. The aerodynamic and mechanical aspects of the WT are modeled using AeroDyn [14] and FAST [15] codes considering component dynamics. The turbine is connected to the SCIG, modeled in MATLAB/Simulink. The equations describing the dynamics of the induction machine can be written as follows [16]:

$$L_m \frac{d}{dt}[(1+\delta_s)\vec{i_s} + e^{j\theta_r}\vec{i_r}] = \vec{V_s} - R_s\vec{i_s} \quad (1)$$

$$L_m \frac{d}{dt}[(1+\delta_r)\vec{i_r} + e^{-j\theta_r}\vec{i_s}] = \vec{V_r} - R_r\vec{i_r} \quad (2)$$

where δ_s and δ_r are the stator and rotor leakage factors, defined as follows:

$$\delta_s = \frac{L_s}{L_m} - 1 \quad (3)$$

$$\delta_r = \frac{L_r}{L_m} - 1 \quad (4)$$

The machine electrical torque can be derived as follows:

$$T_e = (1.5PL_m)\,\mathrm{Im}\{e^{-j\theta_r}\vec{i_s}\vec{i_r}^*\} \quad (5)$$

The rotor speed-torque relation can be written as follows:

$$\frac{d}{dt}\omega_r = \frac{P}{J}(T_e - T_m) \quad (6)$$

$$\frac{d}{dt}\theta_r = \omega_r \quad (7)$$

where L_s, R_s are the stator inductance and resistance, L_r, R_r are the rotor inductance and resistance, respectively. $\vec{V_s}$, $\vec{V_r}$ are the stator and rotor voltage vectors, $\vec{i_s}$, $\vec{i_r}$ are the stator and the rotor current vectors, δ_s and δ_r are the stator and rotor leakage factors, L_m is the magnetizing inductance, P is the pole numbers, ω_r is the rotor angular electrical speed, J is the generator and shaft inertia, T_e and T_m are the electrical and mechanical torques, and θ_r is the rotor angular electrical position.

The generator and rotor side converters are modeled as voltage-sourced average models. The control signals are applied to the converters to achieve satisfactory results as will be discussed in Section III.

B. Simulation Platform

A wind turbine is a complex system consisting of different aspects such as aerodynamic, mechanical, electrical, and control sub-systems. A simulation platform capable of considering these parts and the interaction between them is therefore required. The platform used for this work combines different software packages including TurbSim [17], AeroDyn, FAST and MATLAB/Simulink to develop a comprehensive model for wind energy conversion systems (WECSs). This software platform allows for the study of the interaction of the electrical and mechanical parts of a WT using wind profile information and the study of the implementation of various control configurations.

The master simulation platform is MATLAB/Simulink where FAST equations of motion are implemented as an S-function in Simulink. AeroDyn is called up in FAST as a subroutine to calculate the aerodynamic forces based on blade element momentum (BEM) theory and the results are returned to FAST for mechanical calculations. A wind profile should be given to the AeroDyn subroutine for aerodynamic calculations. TurbSim, a turbulent, full-field and stochastic wind simulator, is used to generate a wind profile. This software requires wind turbine specifications and some meteorological boundary conditions to simulate time series of wind velocity vectors at different points of a two-dimensional vertical rectangular grid.

FAST can model the dynamic response of three-bladed horizontal axis WTs; it can consider different configurations

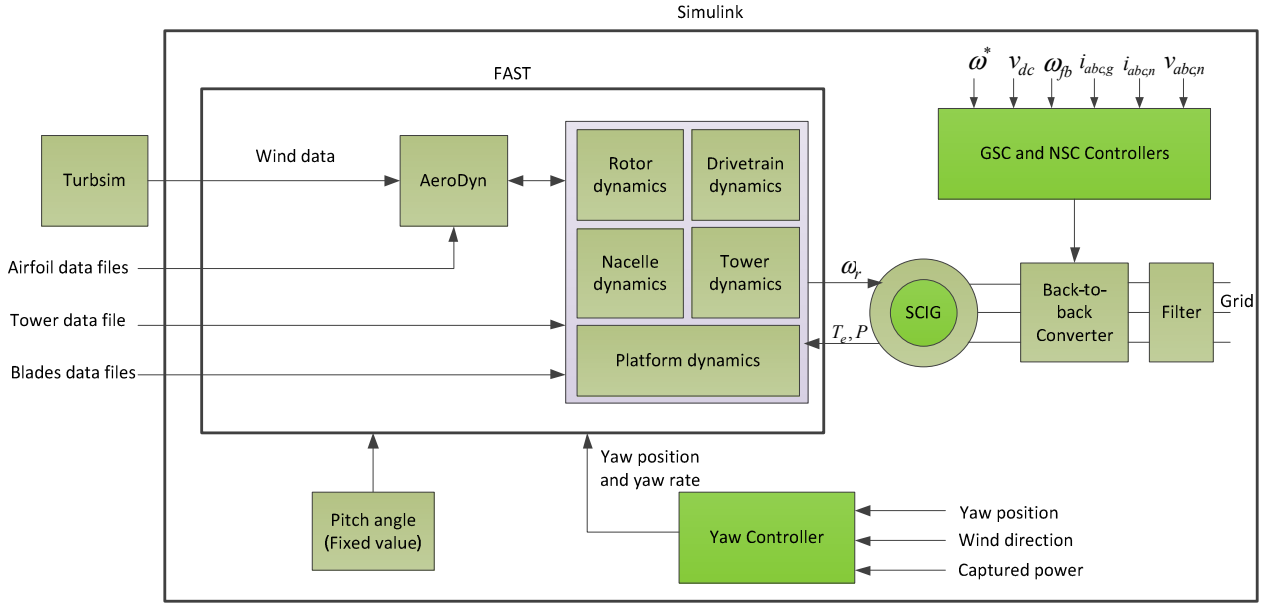

Fig. 2. Simulation platform of a wind energy conversion system

and up to 24 degrees of freedom (DOFs) using a combined modal and multi-body dynamics formulation. These DOFs, which can be activated based on problem requirements, include support platform, tower, blades, yawing motions, rotor- and tail-furl, generator azimuth angle, and the compliance in the drivetrain between the generator and hub/rotor. The result of FAST, either the rotor speed or mechanical torque, is fed to the induction generator modeled in Simulink, where the electrical and mechanical controllers, power electronic interface and power system are implemented. Simulink returns the electromagnetic torque, electrical power, yaw and pitch angle (if necessary) to FAST for the next step of the simulation. This process is repeated until the simulation has been completed. A block diagram of the complete simulation platform is shown in Fig. 2.

III. Control Systems

The control systems in this study can be divided into electrical and mechanical sub-systems. The electrical controller, associated with the power electronics interface, and the mechanical controller, related to the yaw mechanism, will be discussed in the following sections.

A. Power Electronics Interface Control Design

The wind turbines are connected to the AC grid through a generator side converter (GSC), a network side converter (NSC), a filter and cabling. The GSC and NSC are averaged model voltage sourced and are controlled independently in the *d-q* reference frame.

1) Generator side converter (GSC) control

The SCIG can be controlled using methods such as direct field oriented control (FOC), indirect FOC, and direct torque control (DTC); in this paper, indirect FOC is used to control the SCIG via the GSC. The GSC controller (Fig. 3(a)) has control loops to track the torque command (T_e^*) and reference flux (λ^*), by *q* and *d* components of the stator currents (i_{sq} and i_{sd}), respectively. The torque command is the output of the rotor speed control loop that is used to track the maximum power point; the reference flux is set to the machine rated flux. Since the indirect FOC method is used to control the GSC, the flux observer is required to determine the machine magnetizing current ($\hat{i}_{mr}$), stator angular frequency (ω), and *d-q* frame synchronization angle (ρ). The flux observer (Fig. 3(b)) and GSC have been designed based on [16]. The flux observer is based on the following equations:

$$\omega = \frac{d\rho}{dt} \tag{8}$$

$$\tau_r \frac{d}{dt}\hat{i}_{mr} = -\hat{i}_{mr} + i_{sd} \tag{9}$$

$$\omega = \omega_r + \frac{i_{sq}}{\tau_r \hat{i}_{mr}} \tag{10}$$

where τ_r is the rotor time constant as follows:

$$\tau_r = \frac{(1+\delta_r)L_m}{R_r} \tag{11}$$

The controller output voltage signals, applied to the voltage-sourced converter, can be obtained as follows:

$$m_d = \frac{2R_s[u_d - \delta\tau_s\omega i_{sq} + (1-\delta)\tau_s \frac{d}{dt}\hat{i}_{mr}]}{v_{dc}} \tag{12}$$

$$m_q = \frac{2R_s[u_q + (1-\delta)\tau_s\omega\hat{i}_{mr} + \delta\tau_s\omega i_{sd}]}{v_{dc}} \tag{13}$$

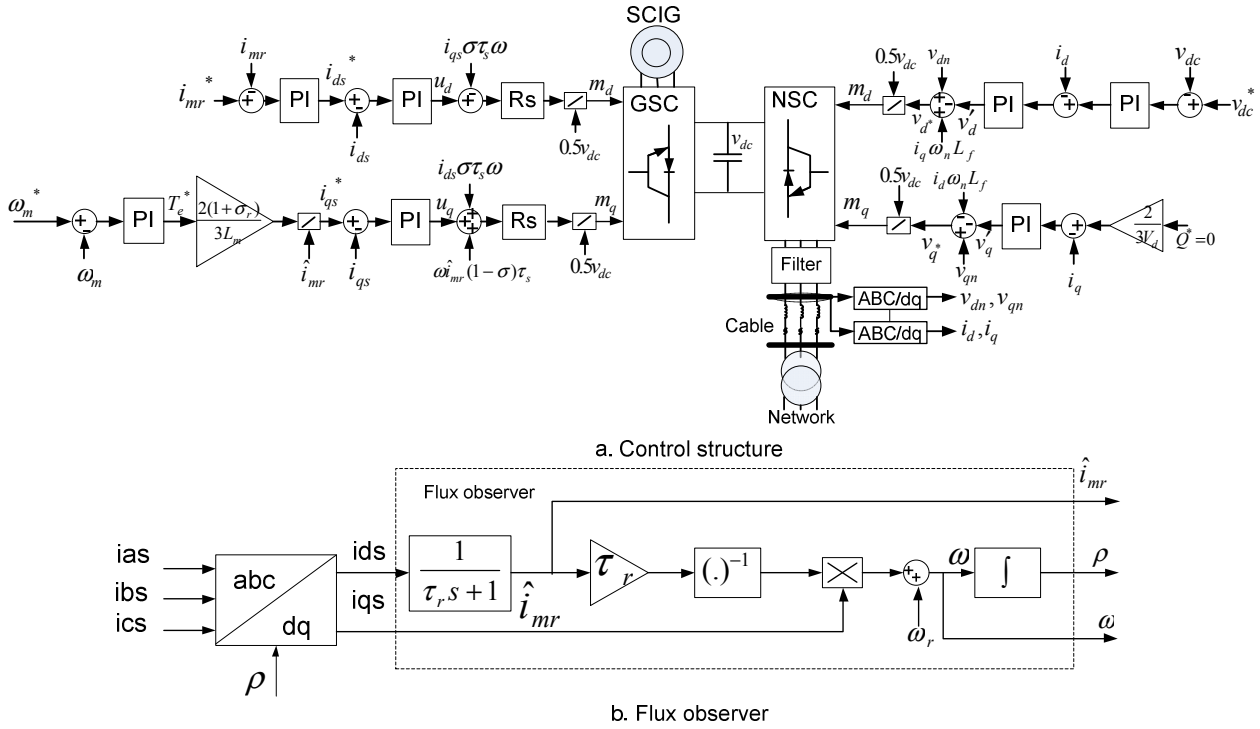

Fig. 3. Power electronic interface controller design and flux observer

where δ is the machine total leakage factor, u_d and u_q are the *d-q* components of the uncompensated voltages, generated by the GSC controller, as follows:

$$u_d = \delta\tau_s \frac{d}{dt} i_{sd} + i_{sd} \tag{14}$$

$$u_q = \delta\tau_s \frac{d}{dt} i_{sq} + i_{sq} \tag{15}$$

$$\delta = 1 - \frac{1}{(1+\delta_r)(1+\delta_s)} \tag{16}$$

The last term in m_d can be ignored to avoid differentiation and possible noise amplification.

2) Network side converter (NSC) control

The NSC controller (Fig. 3(a)) has independent control loops to regulate the DC link voltage and the reactive power to achieve the unity power factor, by *d-q* components of the network currents. The controller output voltage signals applied to the voltage-sourced converter are as follows:

$$m_d = \frac{2}{v_{dc}}(\omega_n L_f i_{qn} - v_d^{'} + v_{dn}) \tag{17}$$

$$m_q = \frac{2}{v_{dc}}(-\omega_n L_f i_{dn} - v_q^{'} + v_{qn}) \tag{18}$$

where i_{dn} and i_{qn} are the *d-q* components of the network currents, v_{dn} and v_{qn} are the *d-q* components of the PCC voltage, R_f and L_f are filter resistance and inductance, ω_n is the network angular frequency, $v_d^{'}$ and $v_q^{'}$ are *d-q* components of the uncompensated voltages, generated by the NSC controller.

B. Stall and Yaw Controller Design

Although stall and yaw-controlled WTs have the same general system configuration and the same control for Region 2 operation, their control differs when the WT operates in Region 3. In Region 2, both WTs track the maximum power point (MPP) by controlling the GSC according to the first (green) part of the rotor speed vs wind speed curve shown in Fig. 4. This curve, which is implemented as a lookup table in the system configuration shown in Fig. 1, is obtained in the design process of the blades or is available from WT manufacturers; it can be generated by HARP_Opt software [18]. In Region 3, the GSC controller (in the stall-controlled WT) operates in the second part of the curve to limit the amount of power extracted from the wind, but the GSC controller in the yaw-controlled WT operates at the rightmost part of the first part of the curve in Fig. 4 and the mechanical yaw controller helps the turbine to limit the extracted power.

In this study, the yaw mechanism rotates the WT toward or out of the wind direction based on the wind speed. When the wind speed is below rated speed, this controller aligns the WT toward the wind direction to reduce the yaw error and extract more energy. On the other hand, when the wind speed exceeds rated speed, this control system rotates the WT out of the wind direction to limit the captured power. When the turbine is rotated out of the wind direction, the effective area swept by the rotor is reduced and thus the captured power is decreased as follows:

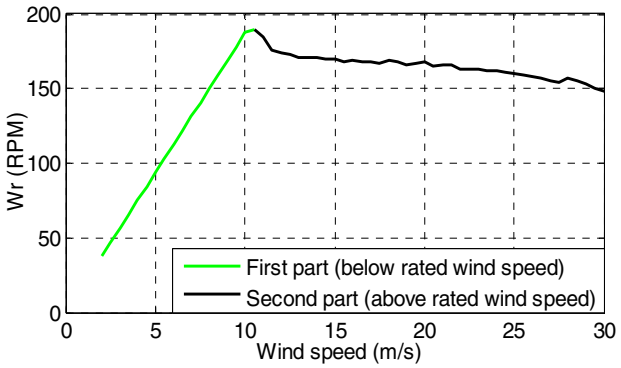

Fig. 4. Rotor speed vs. wind speed lookup table [9]

$$A_{eff} = \pi R_b^2 \times \cos\varphi \tag{19}$$

$$P = 0.5\rho A_{eff} C_p V^3 \tag{20}$$

where A_{eff} is the effective area of the rotor, R_b is the blade length, P is the turbine output power, ρ is air density, C_p is power coefficient, V is wind speed and φ is yaw error as shown in Fig. 5.

IV. Simulation Results

Results of two 10 kW SCIG-based WTs implemented with stall and yaw controls in the simulation platform described in Section II are presented in this section. Fig. 6 shows the turbulent wind profile generated by TurbSim for the analysis of the performance of the two WTs. This wind profile was generated based on the IEC standard [19] with 13 % turbulent intensity and mean wind speed of 16 m/s considering a 6×6 points grid. This profile was selected because the turbulence intensity and mean wind speed were above the rated values; this allowed for the investigation of the performance of the controllers in Region 3 under harsher conditions. The wind turbine, chosen from the FAST CertTest collection (Test 17) [15], and the parameter values of the electrical components used in the simulations are given in Table I and Table II in the Appendix. The rotor speed, mechanical torque, and output power for both WTs are shown in Fig. 7, 8 and 9, respectively.

Both stall-controlled and yaw-controlled WTs have acceptable performance under turbulent wind conditions with the performance of the stall-regulated WT being better. A part of the results are magnified in the figures to see the details of the results. The fluctuations on the output power and torque of the yaw-controlled WT are due to the operation of the yaw controller that rotates the WT out of the wind direction and amplify as yaw error increases.

To analyze flicker emissions, an IEC flickermeter was implemented in MATLAB/Simulink based on [20]. The output voltage, instantaneous flicker sensation (Pfs), and the DC link voltage are also shown in Fig. 10, 11, and 12, respectively. The output voltage fluctuations, instantaneous flicker sensation and dc link voltage oscillations in the stall-regulated WT are less than those in the yaw-regulated WT, proving that power electronic stall control is the superior control method.

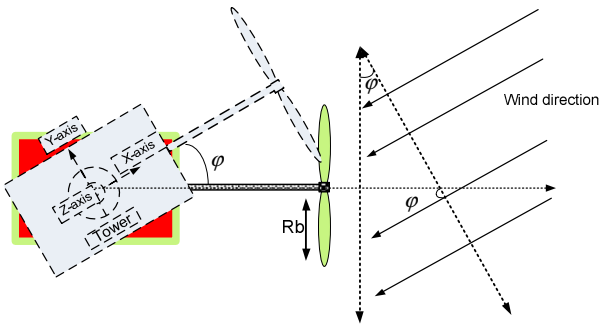

Fig. 5. Yaw mechanism and yaw error (Top view)

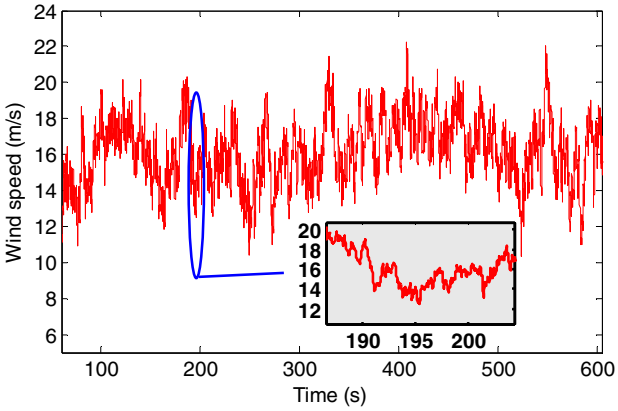

Fig. 6. Wind speed vs. time

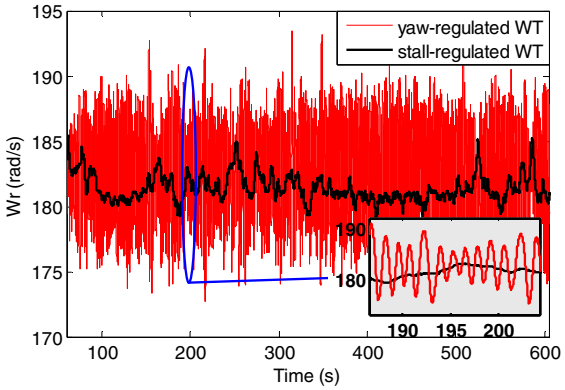

Fig. 7. Rotor speed vs, time

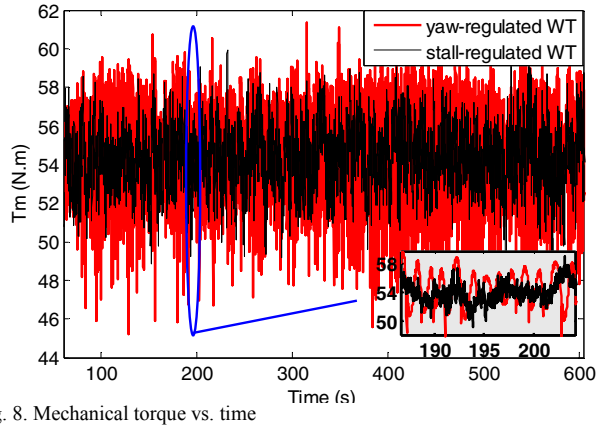

Fig. 8. Mechanical torque vs. time

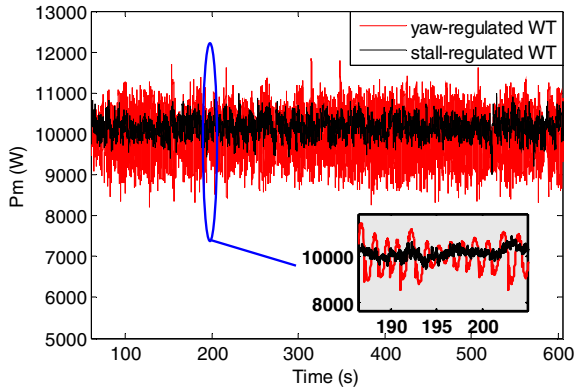

Fig. 9. Output power vs. time

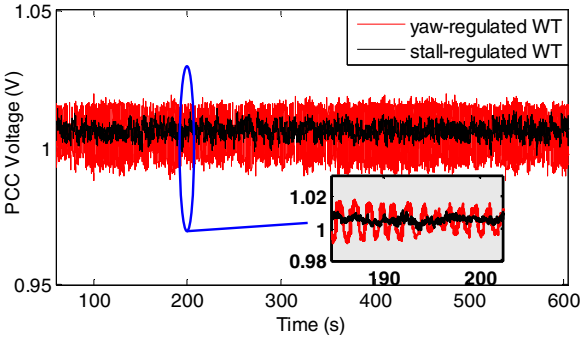

Fig. 10. Point of common coupling (PCC) voltage

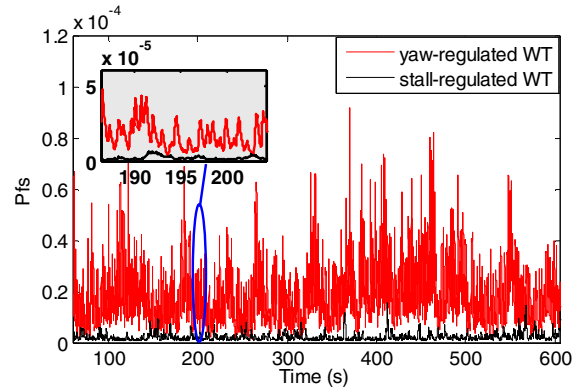

Fig. 11. Instantaneous flicker sensation (Pfs)

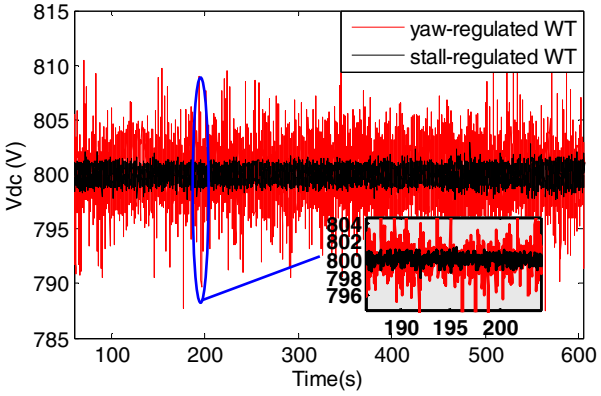

Fig. 12. DC link voltage

V. Conclusion

In this paper, the performance of two control strategies for small-scale variable speed WTs was investigated. In order to have a precise comparison, a comprehensive model of 10 kW WTs that considered electrical, mechanical, and aerodynamic aspects, instead of just one or two which is typically done, was used. In so doing, a simulation platform which combined different software packages was used. TurbSim was used to generate turbulent wind profile, AeroDyn and FAST codes were used to model aerodynamic and mechanical parts, and electrical parts with control systems were implemented in MATLAB/Simulink.

Based on the results obtained, it was shown that the use of power electronics and stall control in WTs can result in improved performance. The fluctuations on the output power and rotor speed of the stall-regulated WT are less than those in the yaw-regulated turbine. Moreover, the stall-regulated WT has better performance in terms of voltage fluctuation and instantaneous flicker sensation comparing to the yaw-regulated turbine.

References

[1] D. Wood, Small Wind Turbines Analysis, Design, and Application, London: Springer, 2011.

[2] H. Li, K. L. Shi and P. G. McLaren, “Neural-network-based sensorless maximum wind energy capture with compensated power coefficient,” IEEE Trans. Ind. Appl, vol. 41, no. 6, pp. 1548-1556, Nov. 2005.

[3] R. Hilloowala and A. M. Sharaf, “A rule-based fuzzy logic controller for a PWM inverter in a stand alone wind energy conversion scheme,” IEEE Trans. Ind. Appl, vol. 32, no. 1, pp. 57–65, Jan. 1996.

[4] K. H. Kim, T. L. Van, D. C. Lee, H. S. Song, and E. H. Kim, "Maximum output power tracking control in variable-speed wind turbine systems considering rotor inertial power," IEEE Trans. Ind. Electron, vol. 60, no. 8, pp. 3207-3217, Aug. 2013.

[5] J. S. Thongam, and M. Ouhrouche, MPPT Control Methods in Wind Energy Conversion Systems, Croatia: InTech Open Access Publisher, 2011.

[6] D. Kumar, and K. Chatterjee, "A review of conventional and advanced MPPT algorithms for wind energy systems." Renewable Sustainable Energy Rev, vol. 55, pp. 957-970, March 2016.

[7] E. Muljadi, and C. P. Butterfield, “Pitch-controlled variable-speed wind turbine generation,” IEEE Trans. Ind. Appl, vol. 37, no. 1, pp. 240-246, Jan. 2001.

[8] H. Shariatpanah, R. Fadaeinedjad, and M. Rashidinejad, “A new model for PMSG-based wind turbine with yaw control,” IEEE Trans. Energy Convers, vol. 28, no. 4, pp. 929-937, Sept. 2013.

[9] H. Shariatpanah, R. Fadaeinedjad, and G. Moschopoulos, “An investigation of furl control in a direct-drive PMSG wind turbine,” in 2014 IEEE 36th International Telecommunications Energy Conference (INTELEC), 2014, pp. 1-8.

[10] E. Muljadi, K. Pierce, and P. Migliore, “Soft-stall control for variable-speed stall-regulated wind turbines,” J. Wind Eng. Ind. Aerodyn, vol. 85, no. 3, pp. 277-291, Apr. 2000.

[11] J. M. Jonkman, and A. Craig Hansen, “Development and validation of an aeroelastic model of a small furling wind turbine,” in the 43rd AIAA Aerospace Sciences Meeting and Exhibit, 2005, pp. 1-11.

[12] E. Muljadi, T. Forsyth, and C. P. Butterfield, “ Soft-stall control versus furling control for small wind turbine power regulation,” National Renewable energy Laboratory (NREL), Tech. Rep, no. CP-500-25100, Golden, CO (United States), 1998.

[13] E. Mohammadi, R. Fadaeinedjad, H. Shariatpanah, and G. Moschopoulos, “Performance evaluation of yaw and stall control for small-scale variable speed wind turbines,” in 2017 IEEE 30th Canadian

Conference on Electrical and Computer Engineering (CCECE), 2017, pp.1-4.

[14] P. J. Moriarty, A. C. Hansen, AeroDyn theory manual. National Renewable Energy Laboratory (NREL), Golden, CO, USA, Tech. Rep. TP-500-36881, Jan. 2005.

[15] J. M. Jonkman , M. L. Buhl M L, FAST user's guide. National Renewable Energy Laboratory, Golden, CO, Tech. Rep. EL-500-38230, Aug. 2005.

[16] A. Yazdani, and R. Iravani, Voltage-Sourced Converters in Power Systems: Modeling, Control, and Applications, New Jersy: John Wiley & Sons, 2010.

[17] B. J. Jonkman , TurbSim user's guide: Version 1.50, National Renewable Energy Laboratory (NREL), Golden, CO, USA, Tech. Rep. Sept. 2012.

[18] D. C. Sale, HARP_Opt User's Guide, National Renewable Energy Laboratory (NREL), Golden, CO, USA, Tech. Rep, 2010.

[19] IEC 61400-1, Wind turbines-Part 1: Design requirements, 3rd edition. Geneva, Switzerland: International Electrotechnical Commission, Aug. 2005.

[20] A. Bertola, G. C. Lazaroiu, M. Roscia, and D. Zaninelli, "A Matlab-Simulink flickermeter model for power quality studies," in 11th International Conference on Harmonics and Quality of Power, 2004, pp. 734–738.

APPENDIX

The parameter values that were used for the simulation work done for this paper are shown in Tables I and II. Table I shows the parameter values used for the FAST and Aerodyn components of the simulation model and Table II shows the parameter values used for the MATLAB/Simulink component of the model.

TABLE I. WIND TURBINE PARAMETERS

Parameter	Value
Rotor radius	2.9 m
Hub height	34.6 m
Tower height	34 m
Nacelle mass	260.5 kg
Pitch angle	0°
Airfoils for stall-regulated WT	S822, S823,
Airfoils for yaw-regulated WT	SH3052
Cut in wind speed	2 m/s
Nominal wind speed for stall-regulated WT	11 m/s
Nominal wind speed for yaw-regulated WT	12 m/s
Cut out wind speed	30 m/s

TABLE II. ELECTRICAL PARAMETERS

Parameter	Value
Generator rated power	11 kW
Generator rated voltage (line to line)	380 V
Stator resistance	1.2 Ω
Rotor resistance	0.75 Ω
Stator and rotor leakage inductance	0.1781 H
Mutual inductance	0.1694 H
Generator inertia	0.5 $kg.m^2$
Pole pairs	2
DC link capacitance	2500 µf
Switching frequency	3420 Hz
Network rated voltage(line to line)	380 V
X/R ratio	3.6
Network frequency	50 Hz
Filter resistance	0.012 Ω
Filter leakage inductance	0.002 H